Lifetime statistics for a Bloch particle in ac and dc fields

M. Glück, A. R. Kolovsky* and H. J. Korsch
Fachbereich Physik, Universität Kaiserslautern, D-67653 Kaiserslautern, Germany
(December 14, 1998)

We study the statistics of the Wigner delay time and resonance width for a Bloch particle in ac and dc fields in the regime of quantum chaos. It is shown that after appropriate rescaling the distributions of these quantities have universal character predicted by the random matrix theory of chaotic scattering.

PACS: 03.65.†, 05.45.+b, 73.20Dx

I. INTRODUCTION

Chaotic scattering has been a subject of a rather intensive research activity during the last decade (see, [1–3], and references therein). This phenomenon is encountered in a variety of physical systems ranging from nuclei, atoms and molecules, to mesoscopic ballistic devices and microwave cavities. In this paper we report the results of our study on chaotic scattering of a Bloch particle (a particle in a periodic potential) in the presence of a constant force and a time-periodic driving. Namely, we consider the system with the Hamiltonian

$$H = H_0 + Fx + F_\omega x \cos(\omega t) \ , \qquad (1)$$

$$H_0 = p^2/2 + V(x) \ , \qquad (2)$$

where $V(x)$ is a periodic potential and, to be concrete, we chose $V(x) = \cos x$. The role of the external forces in the Hamiltonian (1) is different: the periodic force typically make the system (classically) chaotic, while the constant force "opens" the system and requires a scattering approach for analyzing it. We present some results of the classical analysis of the system in Sec. II.

The quantum analysis of the system (1) is essentially more subtle. It need not to be mentioned that the Hamiltonian (1) corresponds to a 1D model of a crystal electron in a static and a periodic electric field. Being of very physical importance this model has attracted much attention since the early days of quantum mechanics. Usually the analysis was done by using specific tools of quantum mechanics, without any reference to the classical dynamics. This was actually justified, because the system parameters in the case of crystal electrons correspond to a deep quantum region. The situation has changed recently due to the experiments with semiconductor superlattices [4] and, especially, due to the experiments with neutral atoms in optical lattices [5–8]. For these system the lattice period exceeds that in solid crystals by several orders and the semiclassical region becomes accessible. It is understood, that the chaotic scattering (which is the topic of the present paper) implies the semiclassical region of the parameters. In the notation used it means that the dimensionless Planck constant (entering the momentum operator) is less than unity.

The simplest approach in a quantum-mechanical analysis of the system (1) involves the so-called single-band approximation, i.e., one keeps in consideration only one Bloch band from the whole energy spectrum of the initial Hamiltonian (2). In this way we immediately come to a fundamental notion of the Bloch period $T_B = \hbar/F$, which is a pure quantum quantity. The appearance of a new time period involves the other important characteristic of the system – the condition of commensurability between the Bloch period T_B and the period $T_\omega = 2\pi/\omega$ of the driving force. The properties of the system (1) in a single-band approximation were studied in the papers [9]. It should be realized, however, that a single-band (more generally, N-band) approximation effectively "closes" the system [10]. In fact, the physical mechanism making the system open is the Landau-Zenner tunnelling between the adjacent bands. Correctly taking into account the interband transition is a rather complicated problem, which has been discussed for years (see reviews [11], for example). In Sec. III we describe an approach which overcomes this problem and ensures a system analysis without any approximation [12,13]. We introduce the notion of the effective scattering matrix for the system (1) and identify the number of scattering channels with the dominator q of the commensurability condition $T_B/T_\omega = r/q$ (r, q are coprime integers).

The results of a numerical analysis of the system are presented in Sec. IV. We restrict ourselves by calculating the complex poles of the scattering matrix, i.e., resonances, and the Wigner delay time (the definition of this quantity, characterizing the continuous quasienergy spectrum of the system, is given in Sec. IV). Besides this, we consider only the case of a small number of channels, which is very interesting because of the strong deviation between the quantum and classical dynamics [14,15]. In fact, although the system itself is assumed to be semiclassical ($\hbar < 1$), a small number q of open channels makes it to behave quantum-mechanically. Remembering that $q \sim T_\omega F/\hbar$, it is easy to see that this case corresponds to a weak static force on the level of Planck's constant. [To avoid a misunderstanding we stress that by the term "semiclassical" we mean here only the condition $\hbar < 1$. In some sense this not the fully semiclassical regime. The latter would imply $q \to \infty$ as $\hbar \to 0$.]

The main issue we discuss in this paper is the statistics of the Wigner delay times and resonance widths. It is shown that after an appropriate rescaling the distributions for these quantities have an universal character. The calculated distributions will then be compared with the prediction of the random matrix theory (RMT), thus providing both a test for this abstract theory and a deeper understanding of the features of the system (1).

The random matrix approach is a powerful analytical method in the field of quantum chaos, including chaotic scattering. It is based on the famous conjecture that in the case of chaotic classical dynamics the quantum Hamiltonian can be modeled by a random matrix sharing the same symmetry. General expressions for statistics of many quantities (like delay time or resonance width) were obtained for the case of a Gaussian ensemble of random matrices (see [16] and references therein). We recall some of the known results in Sec. V. Then we define a different (from the commonly used) random scattering matrix. It is based on the circular ensemble instead of the Gaussian one and is an appropriate random scattering matrix for modeling our system of interest. The numerical comparison between the statistics drawn from two different definitions of the random scattering matrices allows us to identify the analytical expressions for the distribution of the resonance width and delay time, against which the result of the preceding section should be compared.

This comparison is given in Sec. VI. We show that the statistics of the Wigner delay time fits the analytical formula pretty well. The statistics of the resonance width also qualitatively coincides with the prediction of RMT. We also study the different symmetries of the Hamiltonian. In fact, it is well known that the prediction of RMT crucially depends on the symmetry class – orthogonal, unitary, or symplectic. It is argued in the paper that the appropriate random matrix ensemble for modeling the properties of the system (1) is the circular unitary ensemble (CUE). In the second part of Sec. VI we briefly consider another dynamical system, which classically has essentially the same dynamics, but possesses a higher symmetry in the quantum case. We show that the difference between two symmetry classes can be well observed in statistics of the Wigner delay time.

II. CLASSICAL DYNAMICS

It is convenient to include the time-periodic term in the Hamiltonian (1) into the Hamiltonian (2) , which is done by the canonical transformation $p \to p + (F_\omega/\omega)\sin(\omega t)$, $x \to x - (F_\omega/\omega^2)\cos(\omega t)$. Then the system Hamiltonian takes the form

$$H = \frac{p^2}{2} + V(x,t) + Fx \ , \qquad (3)$$

where

$$V(x,t) = \cos[x - \epsilon\cos(\omega t)] \ , \quad \epsilon = \frac{F_\omega}{\omega^2} \ . \qquad (4)$$

It is also useful to expand the "new" time-dependent potential $V(x,t)$ in the Fourier series

$$V(x,t) = J_0(\epsilon)\cos x \qquad (5)$$

$$+ \sum_{m=1}^{\infty} J_m(\epsilon)[\cos(x - m\omega t) + (-1)^m \cos(x + m\omega t)] \ ,$$

where $J_m(\epsilon)$ are the Bessel functions. It follows from Eq. (5) that for $F = 0$ the system (3) is a system of many interacting nonlinear resonances and, therefore, its dynamics can be either quasiregular or chaotic depending on a particular choice of the parameters ω and ϵ [17]. Here we restrict ourselves to the same choice $\omega = 10/6$ and $\epsilon = 1.5$ as in the experiment [6], where a developed chaos exists [see Fig. 1(a)].

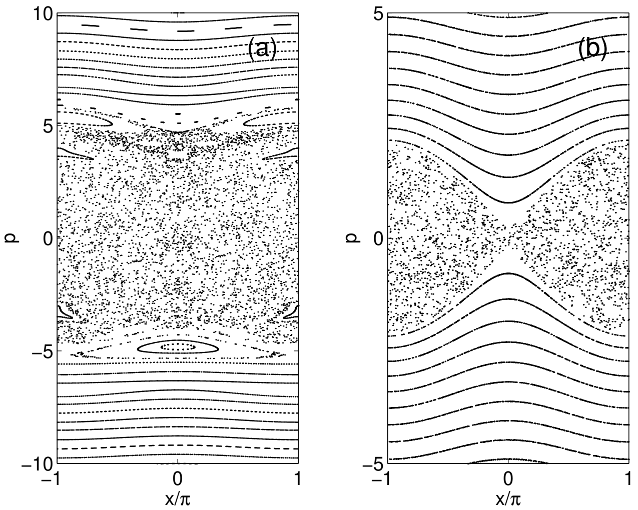

FIG. 1. (a) Phase portrait of the system (3)-(4) for $F = 0$, $\omega = 10/6$, and $\epsilon = 1.5$; (b) Phase portrait of the system (7) for $F = 0$ and $\omega = 0.3$.

Assume now that $F > 0$ and that the initial momentum of the particle well exceeds the value $p^* \approx 5$ corresponding to the boundary between the chaotic and regular component in Fig. 1(a). Then the scattering process consists of three stages: almost uniformly deaccelerated motion for $p > p^*$, temporal chaotic motion for $|p| < p^*$, and accelerated motion for $p < -p^*$ (see Fig. 2). The time spent by the particle in chaotic region is determined by the delay time and randomly varies with the initial condition. We define the classical delay time τ as the time gain or loss relative the case $V(x,t) \equiv 0$. Figure 3 shows the distribution $P_{cl}(\tau)$ of the classical delay time for $F = 0.065$. It is seen that the distribution has an exponential tail

$$P_{cl}(\tau) \sim \exp(-\tau/\tau^*) \ , \qquad (6)$$

which is the "trade mark" of the chaotic scattering. The value of the decay increment τ^* primarily depends on F and for $F=0.13$ and $F=0.065$ (used later on in the quantum simulation) is $\tau^* \approx 0.13F$ and $\tau^* \approx 0.20F$ respectively.

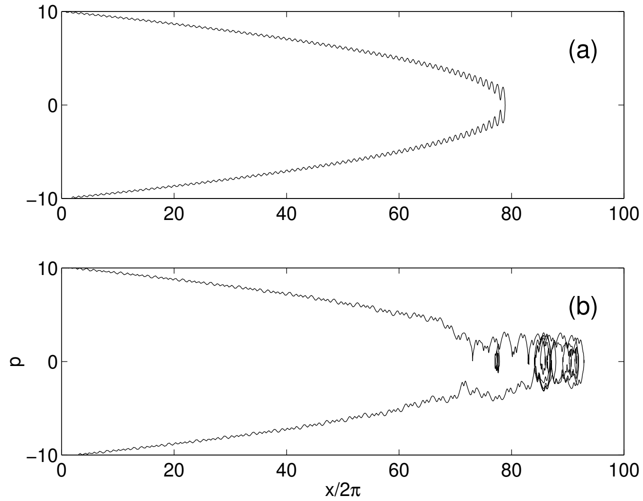

FIG. 2. Example of a classical trajectory for the system (3)-(4) for $F=0.13$, $\epsilon=0$ (a), and $\omega=10/6$, $\epsilon=1.5$ (b).

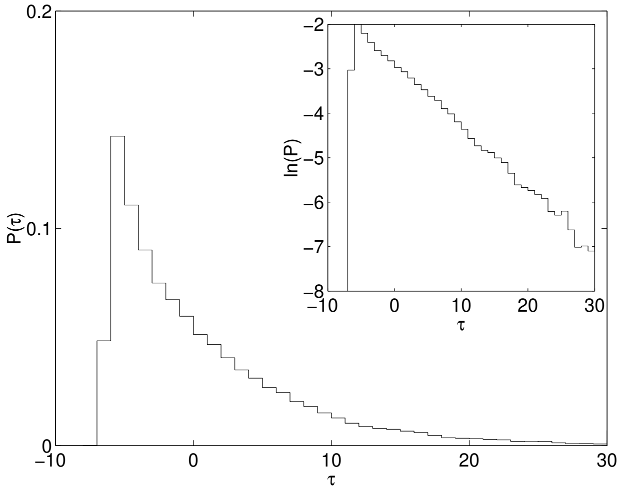

FIG. 3. Distribution of the scaled ($\tau \to F\tau$) classical delay time. The parameters are $F=0.065$, $\epsilon=1.5$, and $\omega=10/6$.

To conclude this section we note that the considered potential (4) is only one of the potentials which can be realized in experiments with optical lattices. In particular in Ref. [7,8] the potential $V(x,t)=f(\omega t)\cos x$ (periodic modulation of laser intensity) was used. The chaotic scattering by this potential is similar to that considered above. In Sec. VI we shall consider the Hamiltonian [18]

$$H=\frac{p^2}{2}+\cos(\omega t)\cos x+Fx\ . \tag{7}$$

The phase portrait for this system is shown in Fig. 1(b) for $F=0$ and $\omega=0.3$. From a theoretical view point the system (7) is preferable to the system(1), because of the simpler structure of the classical phase space. Besides this, it possesses a higher symmetry than the system (1).

III. SCATTERING MATRIX

In this section we introduce the notion of an effective scattering matrix, which relates the asymptotic solution for a quantum particle coming from infinity and scattered back to infinity [13]. The key differences between our approach and the common approach of scattering theory are that the analysis is done in momentum space and that we consider the system evolution operator instead of the system Hamiltonian.

A. Floquet operator

We shall describe the quantum dynamics of the system with help of the evolution operator $\widehat{U}(t)$. In what follows we assume the commensurability condition

$$rT_\omega=qT_B=T\ . \tag{8}$$

(The incommensurate case can then be approached through the limit $r,q\to\infty$, $r/q\to irrational$.) It is proved in Ref. [12] that – provided the condition (8) is satisfied – the system evolution operator possesses the property

$$\widehat{U}(t+T)=\widehat{U}^n(t)\ , \tag{9}$$

and, thus, we can focus on studying the spectral properties of the time-Floquet operator (i.e. evolution operator $\widehat{U}(T)$ over the period T):

$$\widehat{U}(T)\psi(x)=\exp(-i\lambda)\psi(x)\ . \tag{10}$$

We obtain an explicit expression for $\widehat{U}(T)$ by using the standard substitution $\psi(x,t)=\exp(-iFtx/\hbar)\widetilde{\psi}(x,t)$ in the Schrödinger equation, which eliminates the static term in the Hamiltonian (3). Then

$$\widehat{U}(T)=e^{-iqx}\widehat{W}\ , \tag{11}$$

where

$$\widehat{W}=\widehat{\exp}\left\{-\frac{i}{\hbar}\int_0^T\left[\frac{(\hat{p}-Ft)^2}{2}+V(x,t)\right]\mathrm{d}t\right\}\ , \tag{12}$$

and the caret over the exponent denotes time ordering. It is seen from Eqs. (11), (12) that the evolution operator commutes with the translational operator over the lattice period and, therefore, the quasimomentum k is a good quantum number. Presenting the wave function in Eq. (10) in the form

$$\psi(x) = e^{ikx} \sum_{n=-\infty}^{\infty} c_n^{(k,\lambda)} \langle x|n\rangle \ , \quad \langle x|n\rangle = (2\pi)^{-1/2} e^{inx} \ , \tag{13}$$

we reduce the eigenvalue problem (10) to the diagonalisation of an infinite matrix given by the product of two unitary matrices:

$$QW^{(k)}\mathbf{c}^{(k,\lambda)} = \exp(-i\lambda)\mathbf{c}^{(k,\lambda)} \ . \tag{14}$$

In Eq. (14), Q is the shift matrix with the elements

$$Q_{n',n} = \langle n'|\exp(-iqx)|n\rangle = \delta_{n',n-q} \ , \tag{15}$$

and the elements of the matrix $W^{(k)}$ are given by

$$W^{(k)}_{n',n} = \langle n'|\exp(-ikx)\widehat{W}\exp(ikx)|n\rangle \tag{16}$$

$$= \langle n'|\widehat{\exp}\left\{-\frac{i}{\hbar}\int_0^T \left[\frac{(\hat{p} - Ft + \hbar k)^2}{2} + V(x,t)\right] \mathrm{d}t\right\}|n\rangle \ .$$

By convention the expansion coefficients $c_n^{(k,\lambda)}$ are arranged in a column vector $\mathbf{c}^{(k,\lambda)}$ with an index n decreasing from up to down.

We note that quasimomentum k enters Eq. (14) as a parameter. For a general $V(x,t)$ we should scan over k $(-1/2 \le k < 1/2)$ to get the whole spectrum. Excluded is the case of a time independent potential $V(x,t) = V(x)$. In this case the matrices $QW^{(k)}$ are unitarily equivalent and, therefore, the spectrum is degenerate [12]. In what follows, to simplify the formulas, we shall omit the quasimomentum index k and the quasienergy index λ.

B. Scattering matrix, $q = 1$

First we consider the case $q = 1$. The method of solving Eq. (14) is based on the fact that the matrix W tends asymptotically to a diagonal one:

$$W_{n',n} \to \delta_{n',n} w_n \ , \quad n, n' \to \pm\infty \ , \tag{17}$$

$$w_n = \exp\left[-\frac{i}{2\hbar}\int_0^T (\hbar n + \hbar k - Ft)^2 \mathrm{d}t\right] \ .$$

Let us assume that the asymptotic (17) is satisfied "good enough" for $|n| > N$. Then we decompose the vector $\mathbf{c}$ into three sub-vectors

$$\mathbf{c} = \begin{pmatrix} \mathbf{c}^{(+)} \\ \mathbf{c}^{(0)} \\ \mathbf{c}^{(-)} \end{pmatrix} \ , \tag{18}$$

where $\mathbf{c}^{(+)}$ consists of the coefficients c_n with indices $n > N$, $\mathbf{c}^{(-)}$ with $n < -(N+1)$, and $\mathbf{c}^{(0)}$ is constructed from c_n with indices $-(N+1) \le n \le N$. The vector $\mathbf{c}^{(+)}$ is completely specified by the value of the coefficient c_{N+1} and the equation

$$w_n c_n = \exp(-i\lambda)c_{n-1} \ , \tag{19}$$

which follows from Eq. (14) for $q = 1$ and the asymptotic (17). Analogously, the vector $\mathbf{c}^{(-)}$ is specified by Eq. (19) and the value of c_{-N-1}. For the vector $\mathbf{c}^{(0)}$ we have an algebraic equation

$$[B_N - \exp(-i\lambda)]\mathbf{c}^{(0)} = -w_{N+1}c_{N+1}\mathbf{e}_N \ . \tag{20}$$

Here B_N is a matrix of the structure

$$B_N = \begin{pmatrix} \mathbf{0} & 0 \\ W_N & \mathbf{0}' \end{pmatrix} \ , \tag{21}$$

where W_N is the matrix W truncated to the size $(2N+1) \times (2N+1)$, $\mathbf{0}$ and $\mathbf{0}'$ are zero row and column vectors of the length $2N+1$, and $\mathbf{e}_N$ is a column vector of the size $2N+2$ with all elements equal to zero except the first one which is equal to unity. We note that Eq. (20) actually relates the coefficient c_{-N-1} to the coefficient c_{N+1} and, thus, matches two asymptotic solutions $\mathbf{c}^{(+)}$ and $\mathbf{c}^{(-)}$. Without loss of generality we can choose the phase of c_{N+1} such that $-w_{N+1}c_{N+1} = 1$.

We define the matrix $G(\lambda)$ (of dimension 1×1 in the considered case $q = 1$) as a phase gain (loss) relative to the case when the matrix W is given by Eq. (17) for arbitrary n, n' (we shall refer to the latter case as "zero solution"). Thus

$$c_{-N-1} = G(\lambda)\tilde{c}_{-N-1} \ , \tag{22}$$

where $\tilde{c}_{-N-1} \sim \exp[i(2N+2)\lambda]$ is the zero solution. Using Eq. (20), the matrix $G(\lambda)$ can be presented in the form

$$G(\lambda) = \lim_{N\to\infty} a_N(\lambda)\mathbf{e}'_N[B_N - \exp(-i\lambda)]^{-1}\mathbf{e}_N \ , \tag{23}$$

where $\mathbf{e}'_N$ is a row vector with all elements equal to zero except the last one which is equal to unity, and the phase factor $a_N(\lambda) = \tilde{c}^*_{-N-1}$ is given by the zero solution. We also add the limit $N \to \infty$ in the Eq. (23) which insures the validity of the asymptotic formula (17). The numerical calculation of the scattering matrix (23) indicates a rapid convergence for the limit.

C. Scattering matrix, arbitrary q

For arbitrary q, Eq. (19) has the form

$$w_n c_n = \exp(-i\lambda)c_{n-q} \ . \tag{24}$$

It follows from Eq. (24) that there are q independent solutions $\mathbf{c}^{(\pm,i)}$, $(i = 1,\ldots,q)$, and, therefore, the matrix

$G(\lambda)$ is of dimension $q \times q$. We adopt Eq. (23) for this case by substituting the vectors $\mathbf{e}_N$ and $\mathbf{e}'_N$ by a $q \times (2N+1+q)$ matrix e_N and a $(2N+1+q) \times q$ matrix e'_N of the following structure (shown for $q=2$, $N=2$):

$$e_N = \begin{pmatrix} 1 & 0 \\ 0 & 1 \\ 0 & 0 \\ 0 & 0 \\ 0 & 0 \\ 0 & 0 \\ 0 & 0 \end{pmatrix} , \quad e'_N = \begin{pmatrix} 0 & 0 & 0 & 0 & 0 & 1 & 0 \\ 0 & 0 & 0 & 0 & 0 & 0 & 1 \end{pmatrix} . \tag{25}$$

The prefactor a_N is a diagonal $q \times q$ matrix with elements given by the zero solutions. In Eq. (21), defining the matrix B_N, the zero vectors should also be substituted by zero matrices. Below we give a proof that the matrix $G(\lambda)$ constructed this way is explicitly unitary, i.e., $G^+G = \hat{1}$.

First we prove the statement for the matrix $G(\lambda)$ defined as

$$G(\lambda) = e'[B - \exp(-i\lambda)]^{-1} e , \tag{26}$$

$$B = \begin{pmatrix} 0_{M\times N} & 0_{M\times M} \\ A & 0_{N\times M} \end{pmatrix} , \tag{27}$$

where $A = A_{N\times N}$ is an arbitrary unitary matrix and the matrices $e' = e'_{M\times(N+M)}$ and $e = e_{(N+M)\times M}$ have the same structure as in the example Eq. (25). (We note that here we change the notations as $q \to M$ and $2N+1 \to N$. This is done for the sake of comparison with results of Sec.V.) From Eq. (26) we see that the columns of the matrix $G(\lambda)$ are formed by the last M elements of the vectors $\mathbf{c}^i$ satisfying the equation

$$(B - e^{-i\lambda})\mathbf{c}^i = \mathbf{e}^i \tag{28}$$

($\mathbf{e}^i$ is the i-th column of the matrix e). Denoting by $\mathbf{g}^i$ the i-th column of the matrix $G(\lambda)$ and presenting the vector $\mathbf{c}^i$ as

$$\mathbf{c}^i = \begin{pmatrix} \tilde{\mathbf{c}}^i \\ \mathbf{g}^i \end{pmatrix} \tag{29}$$

we obtain from Eq. (28) that

$$\begin{pmatrix} 0_{1,M} \\ A\tilde{\mathbf{c}}^i \end{pmatrix} - \mathbf{e}^i = e^{-i\lambda} \begin{pmatrix} \tilde{\mathbf{c}}^i \\ \mathbf{g}^i \end{pmatrix} \tag{30}$$

Now we take the scalar product of both vectors on the left and right hand sides of equality (30) with those for a different index j:

$$(A\tilde{\mathbf{c}}^i, A\tilde{\mathbf{c}}^j) + (\mathbf{e}^i, \mathbf{e}^j) = (\tilde{\mathbf{c}}^i, \tilde{\mathbf{c}}^j) + (\mathbf{g}^i, \mathbf{g}^j) . \tag{31}$$

Because the matrix A is unitary and $(\mathbf{e}^i, \mathbf{e}^j) = \delta_{i,j}$ we obtain from Eq. (31)

$$(\mathbf{g}^i, \mathbf{g}^j) = \sum_{n=1}^{M} G^*_{n,i} G_{n,j} = \sum_{n=1}^{M} G^+_{i,n} G_{n,j} = \delta_{i,j} . \tag{32}$$

This ends the proof. The extension of this proof to the case of the scattering matrix for a Bloch particle is straightforward because for any finite N it is just the product of the matrix (26) with the diagonal unitary matrix constructed from the coefficients $a_N(\lambda)$.

Besides the relation to the problem currently discussed, the scattering matrix (26) is of its own interest. In Sec. V we shall use the construction (26), (27) to define a random scattering matrix. For the purpose of future use we display one more useful relation, which defines the normalization of the vectors $\mathbf{c}^i$ in Eq. (28). Let us differentiate both side of Eq. (30) with respect to λ. We obtain

$$\begin{pmatrix} 0_{1,M} \\ A\partial_\lambda \tilde{\mathbf{c}}^i \end{pmatrix} = -ie^{-i\lambda}\mathbf{c}^i + e^{-i\lambda} \begin{pmatrix} \partial_\lambda \tilde{\mathbf{c}}^i \\ \partial_\lambda \mathbf{g}^i \end{pmatrix} , \tag{33}$$

where the subindex λ denotes the derivative. Taking the scalar product of Eq. (33) with Eq. (30) we have

$$(A\tilde{\mathbf{c}}^i, A\partial_\lambda \tilde{\mathbf{c}}^j) = -i(\mathbf{c}^i, \mathbf{c}^j) + (\tilde{\mathbf{c}}^i, \partial_\lambda \tilde{\mathbf{c}}^j) + (\mathbf{g}^i, \partial_\lambda \mathbf{g}^j) , \tag{34}$$

or

$$(\mathbf{c}^i, \mathbf{c}^j) = -i \left(G^+ \frac{\mathrm{d}G}{\mathrm{d}\lambda} \right)_{i,j} . \tag{35}$$

D. Complex poles of the scattering matrix

It follows from Eq. (23) that the poles of the scattering matrix $G(\lambda)$ (i.e. the resonances) are the eigenvalues z of the matrix B_N

$$B_N \mathbf{c} = z\mathbf{c} . \tag{36}$$

We note that for any finite N the matrix B_N is *not* unitary and, thus, $|z| \neq 1$. Altogether we have $2N+1-q$ nontrivial solutions of Eq. (36).

One can also take into account the formal limit $N \to \infty$ in Eq. (23). Then Eq. (36) transforms into the equation

$$QW\mathbf{c} = z\mathbf{c} , \tag{37}$$

accompanied by the nonhermitian boundary condition

$$|c_n| \to 0 , \quad n \to \infty , \tag{38}$$

(this should be opposed to the hermitian boundary condition $|c_n| \to 1$, $n \to \pm\infty$ used in the subsection III.2). Obviously, the condition (38) is the so-called resonance boundary condition, corresponding to zero amplitude of the incoming wave. In the case of Eq. (36) it is satisfied automatically.

IV. NUMERICAL RESULTS

In this section we describe the numerical procedure used to calculate the scattering matrix and present some of the numerical results.

A. Quantum resonances

The numerical routine (based on the scientific package MATLAB) is organized in the following way. We write the Hamiltonian $\widetilde{H}(t) = (\hat{p} - Ft + \hbar k)^2/2 + V(x,t)$ in the exponent of Eq. (16) in the basis of the functions $\langle x|n\rangle$, truncate it to the size $(2N+1)\times(2N+1)$, and calculate the operator exponent as the product of infinitesimal propagators

$$W_N = \prod_{i=1}^{N_t} \exp\left[-\frac{i}{\hbar}\widetilde{H}_N(t_i)\Delta t\right] \;, \quad \Delta t = T/N_t \;, \quad (39)$$

with $N_t \gg 1$. The result is controlled against the variation of N_t. The characteristic structure of the matrix W_N is shown in Fig. 4 for the classical parameters of Fig. 1(a), $\hbar = 0.5$, and $N = 30$. As expected, the matrix tends to be diagonal in the asymptotic region $|n| > p^*/\hbar$, where $p^* \approx 5$ is the boundary for the chaotic component (see Sec. II). The next stage of the numerical procedure is the construction of the nonunitary matrix B_N (21) which is followed by its diagonalisation. To obtain the whole spectrum, the calculation is repeated for every value of k (with the step $\Delta k = 1/200$) in the first Brillouin zone.

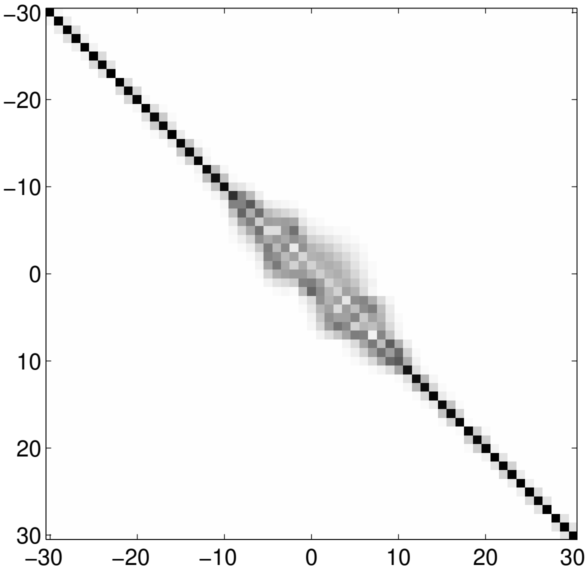

FIG. 4. Characteristic structure of the matrix (16). Parameters are $\omega = 10/6$, $\epsilon = 1.5$, $\hbar = 0.5$, and $F = \hbar/T_\omega \approx 0.13$.

The resulting complex spectrum is depicted in Fig. 5 in polar coordinates for $q = 1$ [Fig. 5(a), see also Fig. 6(b)] and $q = 2$ [Fig. 5(b)]. The parameters are $\omega = 10/6$, $\epsilon = 1.5$, $\hbar = 0.25$, $F = q\hbar/T_\omega$, $N = 31$, $N_t = 32$. It is seen that the spectrum consists of two parts – the resonances associated with the chaotic component (the central part of the matrix W_N) are concentrated close to the unit circle, while the broad resonances associated with outer regular regions (asymptotic part of W_N) are located in the central part of the circle. By increasing N, new such resonances appear in the center. (The positions of the broad resonances already found can be also essentially corrected.) These broad resonances are of little physical interest and we take them out of consideration in the further analysis.

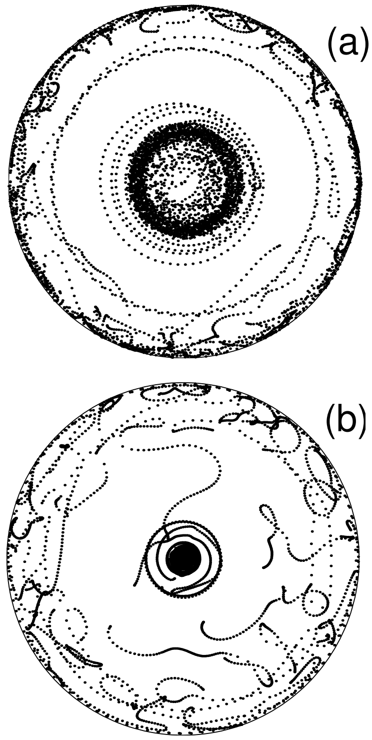

FIG. 5. Complex quasienergy spectrum of the system in (a) the one-channel case $F = \hbar/T_\omega$ and (b) the two-channel case $F = 2\hbar/T_\omega$. The quasimomentum k is scanned over the first Brillouin zone with a step $\Delta k = 1/200$. The truncation parameter $N = 31$.

B. Wigner delay time

An important characteristic of the scattering process is the quantity

$$\tau = -\frac{i}{q}\frac{\mathrm{d}\ln[\det G(\lambda)]}{\mathrm{d}\lambda} \;, \quad (40)$$

which is known in the literature as the Wigner delay time (the quantum analog of the classical delay time) and is directly related to the density of states of a continuous quasienergy spectrum. Another expression for the Wigner delay time has the form

$$\tau = \frac{1}{q}\mathrm{Tr}(\hat{\tau}) \ , \tag{41}$$

where

$$\hat{\tau} = -iG^{+}\frac{\mathrm{d}G}{\mathrm{d}\lambda} \ , \tag{42}$$

is the Smith matrix [19].

A nice feature of the delay time is its stability against an increase of the size of the matrix W_N in Eq. (21). This is due to the fact that the broad resonances (progressively appearing with increase of N) are located far from the real axis and, therefore, their contribution to the functional dependence $G(\lambda)$, λ real, is negligible. This explains the rapid convergence of the limit in Eq. (23). We also note that the diagonal elements of the matrix (42) determine the normalization of the sub-vector $\mathbf{c}^{(0,i)}$. [The whole vector $\mathbf{c}_{\lambda}^{(i)}$ is normalized against a δ-function: $\langle \mathbf{c}_{\lambda'}^{(i)} | \mathbf{c}_{\lambda}^{(j)} \rangle = \delta_{i,j}\delta(\lambda' - \lambda)$.] Namely,

$$\tau_{i,i} = \lim_{N\to\infty} \sum_{n=-N-q}^{N} (|c_n^{(0,i)}|^2 - 1/q) \ . \tag{43}$$

A proof of this equation is in line with proving Eq. (35) in Sec. III. A calculation of the delay time τ on the basis of Eq. (43) and Eq. (41) is actually preferable compared to Eq. (40) because it eliminates a numerical estimation of the derivative.

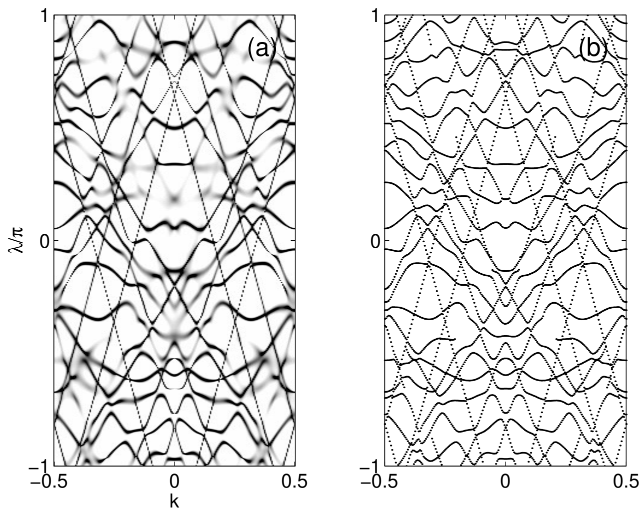

FIG. 6. (a) Delay time $\tau = \tau(\lambda, k)$ in the one-channel case. The limits of the gray-color map are set $-8 \le \tau \le 40$, i.e., absolute black color corresponds to $\tau > 40$, white color corresponds to $\tau < -8$. (b) Real part of the complex quasienergy spectrum. Only the 25 most stable states are plotted for each k.

The left panel in Fig. 6 shows the delay time τ as a function of the quasienergy λ and the quasimomentum k for the parameters of Fig. 5(a). In addition, the right panel in Fig. 6 depicts the real part of the complex quasienergies corresponding to the most stable states. As expected, the delay time $\tau = \tau(\lambda, k)$ reveals the underlying resonance structure. For the two-channel case, $q = 2$, the Wigner delay time is shown in Fig. 7 together with the proper delay time $\tau_{1,1}$ (a diagonal element of the Smith matrix). It is seen that the Wigner delay time is symmetric with respect to inversion of k, but the proper delay time is not.

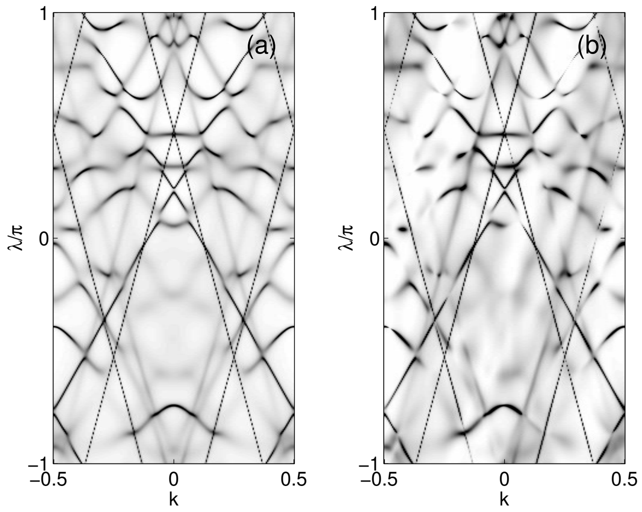

FIG. 7. Delay time in the two-channel case: (a) Wigner delay time $\tau = (\tau_{1,1} + \tau_{2,2})/2$; (b) diagonal element $\tau_{1,1}$ of the Smith matrix.

To conclude this section we would like to draw the attention of the reader to the regular structure in the straight lines with the slope ± 2 in Figs. 6-7, and the circles in Fig. 5. This structure results from the stability islands of classical phase space and can be determined by using a specific perturbation theory [14]. Apart from this regularity, the structure of the delay times and the complex spectrum looks pretty chaotic. In Sec. VI we calculate the distribution functions for the Wigner delay time and the resonance width and compare them with the prediction of random matrix theory.

V. RANDOM MATRIX APPROACH

A. Hamiltonian based random scattering matrix

We recall some of the results of the random matrix approach to chaotic scattering [3,16,20–22]. Nowadays, the random matrix approach is mainly based on the following definition of a random scattering matrix $S(E)$

$$S(E) = I - 2\pi V^{+}(H_{\mathrm{eff}} - E)^{-1}V \ , \tag{44}$$

$$H_{\rm eff} = H - i\pi V V^{+} \ . \qquad (45)$$

In Eqs. (44), (45) H is a $N\times N$ random matrix belonging to the GOE or GUE universality classes and V is a $N\times M$ coupling matrix satisfying the orthogonality condition

$$\sum_{i=1}^{N} V_{i,a}^{*} V_{i,b} = (g_a/\pi)\delta_{a,b} \ .$$

The coupling constants g_a are input parameters of the model. It can be shown that their values define the ensemble averaged diagonal elements of the scattering matrix

$$\langle S_{a,a}(E)\rangle = \frac{1-g_a f(E)}{1+g_a f(E)} \ , \quad f(E) = iE/2 + \sqrt{1-E^2/4} \ , \qquad (46)$$

which is an important characteristic in physical applications. (The function $f(E)$ is related to the density of states of the system (45), which depends on the energy E.) A matrix of the form (44) naturally appears, for example, in the problem of electron scattering in a mesoscopic cavity [3,20,21]. Then the random Hamiltonian H models N eigenstates of the cavity and M is number of open channels at the energy E in a lead connecting the cavity with a bath of an electron gas.

Knowing the statistical properties of the hermitian (symmetric for GOE) matrix in Eq. (44), the distribution for the resonance widths and the distribution for a partial delay time $\tau_i = {\rm d}\theta_i/{\rm d}E$ [$\theta_i=\theta_i(E)$ are the eigenphases of the matrix $S(E)$] can be obtained [16]. In the case $N \gg M$, GUE universality class, and equivalent channels ($g_a = g$) these distribution are

$$P(\tau_s) = \frac{(-1)^M}{\pi M! \tau_s^{M+2}} \qquad (47)$$

$$\frac{\partial^M}{\partial(\tau_s^{-1})^M}\left[\exp(-\kappa\tau_s^{-1}) I_0(\tau_s^{-1}\sqrt{\kappa^2-1})\right] \ ,$$

for the scaled partial delay time $\tau_s = \tau\Delta/2\pi$ (Δ is the mean level spacing), and

$$\Pi(\Gamma_s) = \frac{(-1)^M}{(M-1)!}\Gamma_s^{M-1}\frac{d^M}{d\Gamma_s^M}\left(e^{-\kappa\Gamma_s}\frac{\sinh\Gamma_s}{\Gamma_s}\right) \ , \qquad (48)$$

for the scaled resonance width $\Gamma_s = \pi\Gamma/\Delta$. In Eqs. (47), (48) $I_0(z)$ denotes the modified Bessel function and

$$\kappa = \frac{1}{2{\rm Re}f(E)}\left(g+g^{-1}\right) \ , \qquad (49)$$

i.e., the distributions are symmetric with respect to $g \to 1/g$.

We also note the relation between the distributions of the resonance width $\Pi(\Gamma_s)$ and distribution $\tilde{P}(\gamma_s)$ of the inverse delay time $\gamma_s = 1/\tau_s$

$$\Pi(x) \sim \tilde{P}(x)/x \ , \quad x \ll 1 \ , \qquad (50)$$

which seems to be universal [22]. A remarkable feature of the distributions (47), (48) is the existence of an algebraic tail for both the delay time τ and decay time $\tau' = 1/\Gamma$. Physically it means that an electron "can be captured by the cavity" for very long time, if we have this particular problem in mind.

B. Evolution operator based scattering matrix

One can question whether the results (47) and (48) can be applied to our system of interest. In fact, in our case the system Hamiltonian has a "regular" structure and only the evolution operator can be considered as "random" in some sense. Besides, the argument of our efficient scattering matrix is a quasienergy (defined in the interval $-\pi<\lambda<\pi$) but not an energy. This would require a random matrix theory of scattering based on the circular ensemble instead of the Gaussian one. A definition of such a random scattering matrix can be given by using Eqs.(26)-(27), where we just substitute the matrix A by a random CUE matrix.

In the absence of an analytical theory for the statistics of the delay time τ and resonance width Γ of random scattering matrices based on CUE, we find them numerically. The result is compared with distributions (47), (48) where we chose $f(E)\equiv 1$ and $\kappa = 1$. The reason for this choice of $f(E)$ is that in our case the density of states is uniform [with mean quasienergy level spacing $\Delta = 2\pi/(N-M)$]. The formal reason for the particular choice $\kappa=1$ is the numerical evidence that $\langle G_{a,a}(\lambda)\rangle = 0$ [see Eqs. (46), (49)]. We note that in the case $\kappa=1$ the formula (47) simplifies to

$$P(\tau_s) = \frac{1}{M!}\frac{1}{\tau_s^{M+2}}\exp\left(-\frac{1}{\tau_s}\right) \qquad (51)$$

and the distribution (48) gains quite a specific feature as the power tail for large resonance width

$$\Pi(\Gamma_s) \sim \frac{M}{2\Gamma_s^2} \ , \quad \Gamma_s \gg 1 \ . \qquad (52)$$

Three smooth curves in Fig. 8 show the distribution of the scaled resonance width for GUE based scattering matrix for $\kappa = 1$ and $M = 1,2,3$ [see Eq. (48)]. We calculated the distribution of the resonance width for a CUE based scattering matrix for these three cases and found a perfect coincidence. As an example, we depict in Fig. 8 the histogram for the normalized width $\Gamma \to \pi\Gamma/\Delta = \Gamma(N-M)/2$ for $M=1$. The statistical ensemble involves 5000 CUE matrices of the size $N=41$ [23].

We proceed with the delay time. We find it is more convenient to study the distribution of the diagonal elements $\tau_{i,i}$ of the Smith matrix (42) (the proper delay time) than the distribution of the partial delay time

$\tau_i = \mathrm{d}\theta_i/\mathrm{d}\lambda$. The distributions for these quantities are expected to be essentially the same. We also note the obvious relation

$$\frac{1}{M}\sum_{i=1}^{M}\tau_{i,i} = \frac{1}{M}\sum_{i=1}^{M}\tau_i \equiv \tau \quad , \ \tau_i = \frac{\mathrm{d}\theta_i}{\mathrm{d}\lambda} \ . \qquad (53)$$

Because the proper (partial) delay times are not independent variables, the distribution for the Wigner delay time τ is not a convolution of the distribution for the proper (partial) times. On the contrary, we found that (at least for $M \leq 3$) the distribution for the Wigner delay time to be close to that of the proper delay time.

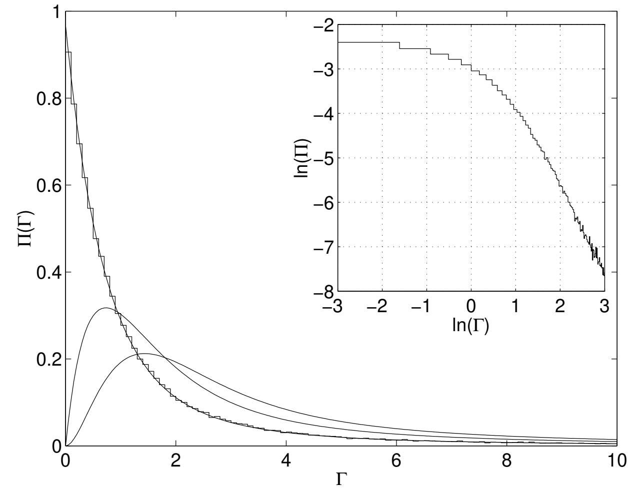

FIG. 8. The histogram shows distribution of the scaled resonance width for the scattering matrix (26)-(27) with a matrix A belonging to CUE. Dimension of the matrix A is $N = 41$, number of channel $M = 1$. Solid lines – distribution (48) for $M = 1, 2, 3$ and $\kappa = 1$.

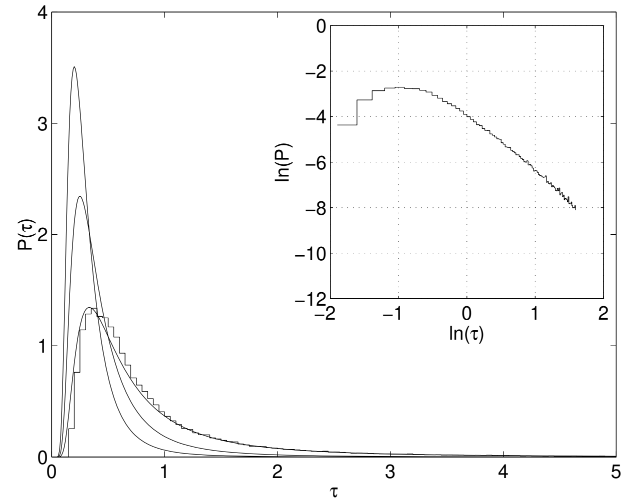

FIG. 9. The same as in the previous figure but for the scaled delay time. The analytical expression is given by Eq. (51).

The histogram in Fig. 9 shows the distribution $P(\tau)$ of the normalized ($\tau \to \tau\Delta/2\pi = \tau/N$) delay time for $M = 1$. This distribution was obtained by generating 50 CUE matrices of the size $N = 41$ and calculating $\tau(\lambda)$ for 4000 equal-distant values of λ. The solid line in the figure corresponds to the function (51) for $M = 1, 2, 3$. A small deviation from the analytical formula is related to a finite matrix size and vanishes with N increased.

The presented numerical results show that the statistics of the delay time and resonance width for random CUE based scattering matrices [i.e., constructed on the basis of Eqs. (26)-(27)] coincides with the statistics for random GUE based scattering matrix (44)-(45) in the case of perfect coupling $\kappa = 1$. An analytical proof of this statement appears to be a challenging problem in the field of random matrix theory.

VI. COMPARISON WITH RMT

In this section we study the statistics of the resonance width Γ and delay time τ for our deterministic system with the Hamiltonian (1). We construct a statistical ensemble by scanning the quasimomentum k with the step Δk over the first Brillouin zone. To have independent representatives of $G(\lambda)$ the step should be of the order of the "correlation length" of the quasienergy bands. Decreasing Δk below this characteristic value neither improves nor spoils the statistics. In our numerical calculation we chose $\Delta k = 1/200$, which is surely less than the correlation length.

A. Unitary symmetry

For a fixed value of k, the evolution operator matrix is generally not invariant with respect to inversion of time. Thus we have the case of unitary symmetry (CUE). An exception are the center $k = 0$ and the edges $k = \pm 0.5$ of the Brillouin zone, where the time-reversal symmetry is preserved. In principle, the vicinity of these points should be excluded from the consideration. However, in the case of a poor statistical ensemble (i.e., the case we have in hand), this procedure may be neglected. A special precaution should be taken by discretising the quasienergy λ. In fact, for $\hbar = 0.25$ the resonances can be as narrow as $\Gamma \sim 10^{-4}$. Thus, not to miss a narrow resonance, the step $\Delta\lambda$ should be small enough. In our calculation we kept $\Delta\lambda = 2\pi/4000$.

The main problem one meets by doing the statistics is an appropriate rescaling of the resonance width and delay time. In fact, we cannot directly use the rescaling formulas from Sec. V

$$\Gamma \to \Gamma(N-M)/2 \approx \Gamma N/2 \ , \quad \tau \to \tau/N \ , \qquad (54)$$

because the notion of the matrix size N is not defined for an infinite matrix (16). One notes, however, that the matrix W has a well pronounced structure [see Fig. 4]. Based on this structure, it looks reasonable to choose the "matrix size" as

$$N = a/\hbar \, , \tag{55}$$

where a is an adjusted parameter of the order of $2p^*$. The other adjusted parameter appears due to the fact that the delay times (43) can be negative for our physical problem (we recall that in the case of RMT $\tau_{i,i}$ is strictly positive). Thus, to compare with RMT, we should shift the distribution of the scaled delay time by some value $b \approx 1/q$.

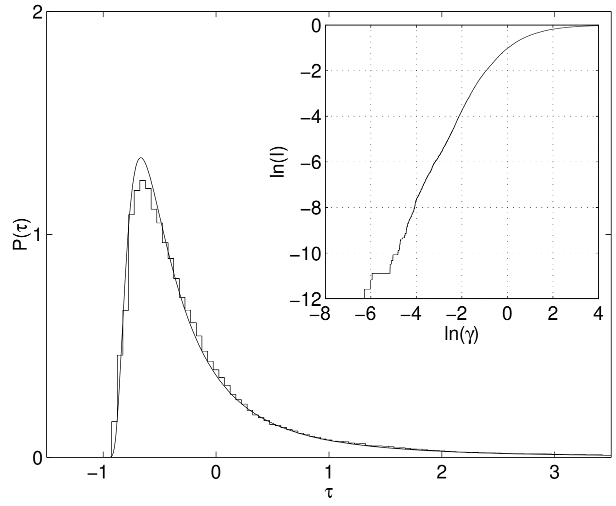

FIG. 10. Distribution of the scaled delay time shown in Fig. 6(a) The insert shows the integrated distribution for the inverse delay time $\gamma = 1/\tau$.

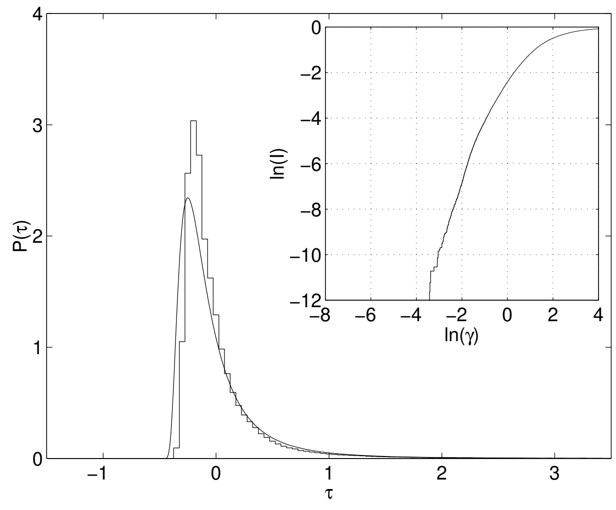

FIG. 11. Distribution of the scaled proper delay time (diagonal element of the Smith matrix) shown in Fig. 7(b).

Figures 10-11 show the distribution of the proper delay time for $q = 1$ and $q = 2$. [Initial data are displayed in Fig. 6(a) and Fig. 7(b), respectively.] The adjusted parameters are $a = 7$, $b = 1$ for the one-channel case ($q = 1$) and $a = 7$, $b = 0.5$ for the two-channel case ($q = 2$). The obtained distributions are compared with Eq. (51), where we shifted the analytical curve instead of shifting the histograms. A nice correspondence is noticed. To be sure about the asymptotic behavior of $P(\tau)$ we also calculated the integrated distribution $\widetilde{P}(\gamma)$ for the inverse delay time $\gamma = 1/\tau$ (negative τ were ignored). The result, shown in the insert, coincides with the prediction of RMT

$$\widetilde{P}(\gamma) \sim \gamma^q \, , \quad I(\gamma) \sim \gamma^{q+1} \, , \quad \gamma \ll 1 \, . \tag{56}$$

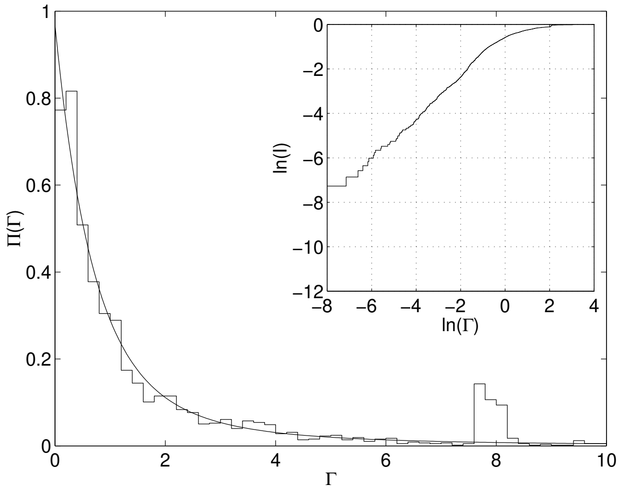

FIG. 12. Distribution of the scaled resonance width in the one-channel case ($q = 1$). Data are drawn from Fig. 5(a), where the resonances with $|z| < 0.45$ are ignored. The insert shows the integrated distribution.

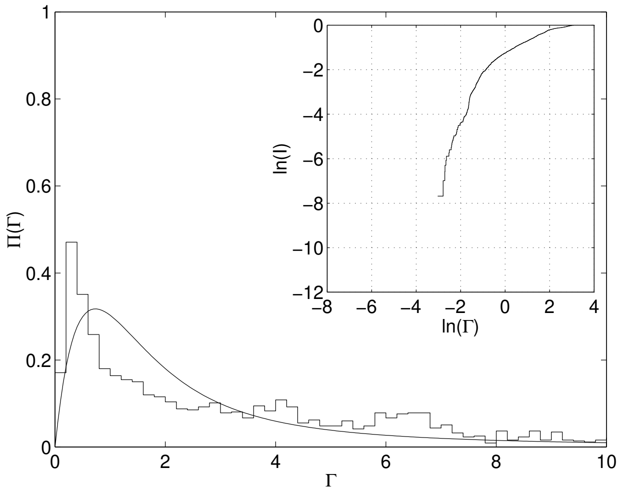

FIG. 13. Distribution of the scaled resonance width in the two-channel case ($q = 2$). Data are drawn from Fig. 5(b).

We proceed with the statistics of the resonance width Γ. The initial data are presented in Fig. 5 where we ignore the resonances with $|z| < 0.45$. As it was mentioned above in Sec. IV, these broad resonances are associated with the outer regular region of classical phase space and can not be studied by using the RMT approach. The histograms for the scaled resonance width (adjusted parameter $a = 7$ is the same) are shown in Fig. 12 for $q = 1$ and Fig. 13 for $q = 2$. Unfortunately, the statistics is not well resolved [24]. Nevertheless, one can see the difference between the one and two channel cases, in qualitative agreement with Eq. (48). (A peak around $\Gamma = 8$ in Fig. 12 is due to stability islands discussed in the concluding paragraph of Sec. IV.)

B. Antiunitary symmetry

Since the prediction of RMT crucially depends on the global symmetry of the system, it is of interest to study different symmetries of the evolution operator (11). The symmetry of the evolution operator reflects itself in the quasienergy spectrum and is actually determined by the symmetry of the potential $V(x,t)$ in the Hamiltonian (3). Above, we have considered the case $V(x,t) = \cos[x - \epsilon\cos(\omega t)]$, where $V(x,-t) = V(x,t)$. In this case the spectrum of the evolution operator is symmetric with respect to the transformation $k \to -k$. In fact, let us present the evolution operator (11) in its k-specific form

$$\widehat{U}^{(k)} = \exp\left(-i\frac{FT}{\hbar}x\right) \tag{57}$$

$$\times\widehat{\exp}\left\{-\frac{i}{\hbar}\int_0^T\left[\frac{(\hat{p}+\hbar k - Ft)^2}{2} + V(x,t)\right]\mathrm{d}t\right\} .$$

Applying time reversal transformation $R: t \to -t$ we see that

$$R: \widehat{U}^{(k)} = \left(\widehat{U}^{(-k)}\right)^* . \tag{58}$$

Thus the eigenfunction $\chi^{(-k,\lambda)}(x)$ of the operator $\widehat{U}^{(-k)}$ is complex conjugate for $\chi^{(k,\lambda)}(x)$ and corresponds to the same quasienergy λ. By noticing that t and k enter Eq. (57) through the combination $\hbar k - Ft$, this symmetry can be easily generalized for $V(x,t) = \cos[x - \epsilon\cos(\omega t + \phi)]$. In this case the point of mirror symmetry is shifted from $k = 0$ to $k = \phi/2\pi$. Excluding the mirror points $k = \phi/2\pi$, $k = \phi/2\pi + 0.5$ this symmetry does not effect the global unitary symmetry and a member of CUE is an appropriate random matrix for modeling the Floquet operator.

Now we consider the potential $V(x,t) = \cos x\cos(\omega t)$ which effects the unitary symmetry of the evolution operator. In addition to the transformation $t \to -t$, this potential is also invariant under the transformation $\widetilde{R}$: $x \to x + \pi$, $t \to t + T_\omega/2$. This invariance leads to a higher symmetry of the evolution operator. Figure 14 shows the delay time (which characterizes the real continuous spectrum) and the discrete complex quasienergy spectrum (only the real part is shown) for the system with the Hamiltonian (7). The parameters are $\omega = 0.3$, $\hbar = 0.25$, and $F = \hbar/T_\omega$. [For $F = 0$ the classical phase portrait of the system is shown in Fig. 1(b).] It is seen that in addition to the symmetry $k \to -k$ the spectrum is also symmetric with respect to the transformation $k \to k + 0.5$, $\lambda \to \lambda + \pi$. Analytically this symmetry is a consequence of the relation

$$\widetilde{R}: \widehat{U}^{(k)} = e^{i\pi}\widehat{U}^{(k+0.5)} . \tag{59}$$

It should be noted that the symmetry (59) is *not* a COE symmetry, because the matrix elements of the evolution operator remain complex. However, it changes the statistics in a way similar to that under the transition from unitary to orthogonal symmetry. By analogy with the problem considered in Refs. [25] we shall refer to this symmetry as antiunitary symmetry.

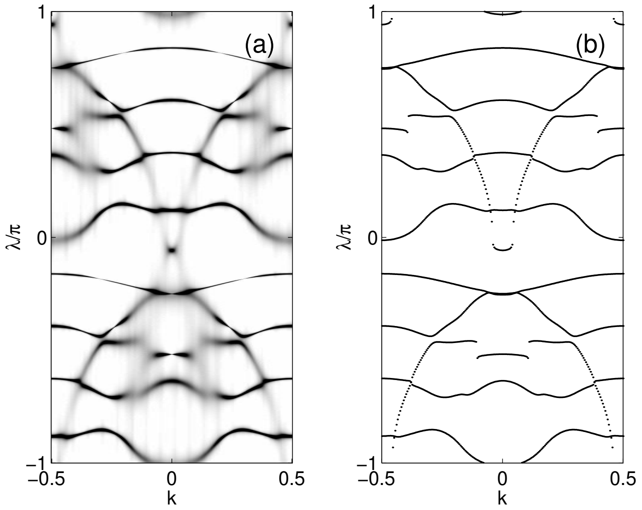

FIG. 14. Delay time as a function of the quasimomentum and quasienergy (a), and real part of the complex quasienergy spectrum (b) for the system (7). Parameters are $\omega = 0.3$, $\hbar = 0.25$, and $F = \hbar/T_\omega$.

The histogram in Fig. 15 shows the distribution of the delay time depicted in Fig. 14. (The delay time was scaled on the basis of Eq. (55) with $a = 3$.) It is seen that this distribution differs essentially from that shown in Fig. 10. We found that now it fits pretty well the formula

$$P(\tau_s) = \frac{(1/2)^{1/2}}{\Gamma(1/2)}\frac{1}{\tau_s^{5/2}}\exp\left(-\frac{1}{2\tau_s}\right) \tag{60}$$

[here $\Gamma(x)$ stands for gamma-function]. Equation (60) is a particular case $\beta = 1$ of a more general expression

$$P(\tau_s) = \frac{(\beta/2)^{\beta/2}}{\Gamma(\beta/2)} \frac{1}{\tau_s^{(\beta+4)/2}} \exp\left(-\frac{\beta}{2\tau_s}\right) \qquad (61)$$

for the distribution of the delay time derived in Ref. [22]. In Eq. (61) $\beta = 1, 2, 4$ corresponds to orthogonal, unitary, and symplectic symmetry, respectively, and a one-channel case is assumed. [Note that in the case $\beta = 2$ considered above Eq. (61) coincides with Eq. (51) for $M = 1$.]

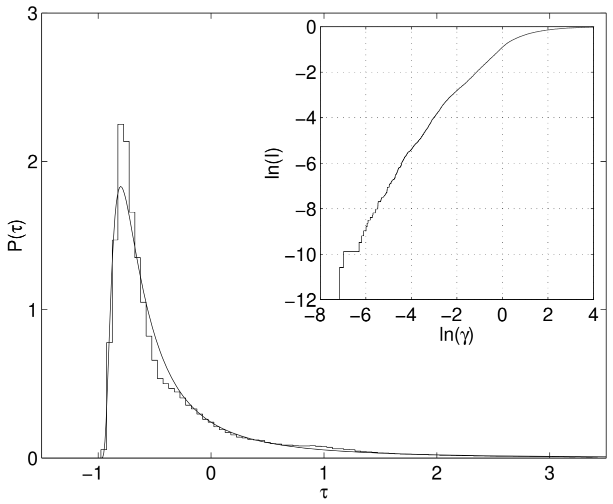

FIG. 15. Distribution of the scaled delay time for the system (7) in the one-channel case. The result is compared with Eq. (61).

VII. CONCLUSION

We have studied the scattering of a quantum particle in a dc field by a space- and time-periodic potential. In the case of a static potential (no time dependence) the resonances are arranged in the complex plane in a regular way, forming the so-called Wannier-Stark ladder of resonances. It is shown in the paper (see also Ref. [14,15]) that the resonance structure is qualitatively different in the case of a time-periodic potential. In this case the classical dynamics of the system is generally chaotic and, as a quantum manifestation of the classical chaos, the location of the resonances is quasi-random. In this case a statistical approach should be and has been applied for describing the resonances.

A fundamental conjecture in the field of quantum chaos is that the distributions of the different quantities characterizing the quantum resonances (like resonance width or delay time) is universal for a chaotic system and depends only on its global symmetry. The analytical expressions for these universal distributions are supplied by the random matrix theory of chaotic scattering. The test of our system of interest against the prediction of RMT (and, in reverse, the test of RMT against our physical system) has been the main subject of this paper.

In the paper we restricted ourselves to the calculation of the resonance width and the Wigner delay time. The numerical procedure was based on a novel method [13] involving the construction of the scattering matrix (23), complex poles of which are the quantum resonances. The calculated resonance widths and delay times were then rescaled on the basis of Eqs. (54)-(55). [The physical meaning of the quantity (55) is the number of states supported by the chaotic component of the classical phase space, i.e., volume of the chaotic component per unit cell divided by $2\pi\hbar$.] We used these data to find the distributions of the resonance widths and delay times, which were compared with the prediction of RMT given by Eq. (48) for the resonance width and Eqs. (51), (59) for the delay time. A striking correspondence was noticed for both cases of unitary ($\beta = 2$) and antiunitary ($\beta = 1$) symmetry. Up to our knowledge, this is the first example, where data calculated for a real physical system fit so well to the prediction of random matrix theory of chaotic scattering.

---

* Also at L. V. Kirensky Institute of Physics, 660036 Krasnoyarsk, Russia.

[1] U. Smilansky, in *Chaos and Quantum Physics*, Proceeding of the Les-Houches Summer School, Session LII, edited by M. J. Giannoni *et. al.* (North Holland, Amsterdam, 1991), p.372.
[2] D. Stone, in *Mesoscopic Quantum Physics*, Proceeding of the Les-Houches Summer School, Session LXI, edited by E. Akkermans *et. al.* (North Holland, Amsterdam, 1995), p.325.
[3] H. A. Weidenmüller, in *Chaos and Quantum Chaos*, edited by W. D. Heiss (Springer, New York, 1992).
[4] E. E. Medez and G. Bastard, Physics Today **46**, No. 6, p.34 (1993).
[5] M. Raizen, C. Solomon, and Qian Niu, Physics Today, No. 7, p.30 (1997).
[6] J. C. Robinson, C. Bharucha, F. L. Moore, R. Jahnke, G. A. Georgakis, Q. Niu, M. G. Raizen, and Bala Sundaram, Phys. Rev. Lett. **74**, 3963 (1995).
[7] F. L. Moore, J. C. Robinson, C. F. Bharucha, Bala Sundaram, and M. Raizen, Phys. Rev. Lett. **75**, 4598 (1995).
[8] K. Vant, G. Ball, H. Ammann, and N. Christensen, Phys. Rev. E (in press).
[9] D. H. Dunlap and V. M. Kenkre, Phys. Rev. B **34**, 3625 (1986); Nguyen Hong Shon and H. N. Nazareno, J. Phys.: Condense Matter **4**, L611 (1992); X.-G. Zhao, R. Jahnke, and Q. Niu, Phys. Lett. A **202**, 297 (1995); K. Drese and M. Holthaus, Phys. Rev. Lett. **78**, 2932 (1997).
[10] J. E. Avron and Zak, J. Math. Phys. **18**, 918 (1977).
[11] J. E. Avron, Ann. Phys. (N.Y.) **143**, 33 (1982); G. Nenciu, Rev. Mod. Phys. **63**, 91 (1991).
[12] M. Glück, A. R. Kolovsky, H. J. Korsch, and N. Moiseyev, EPJ D**4**, 239 (1998).
[13] M. Glück, A. R. Kolovsky, and H. J. Korsch, (unpub-

lished).
[14] M. Glück, A. R. Kolovsky, and H. J. Korsch, Phys. Rev. E **58**, 6835 (1998).
[15] M. Glück, A. R. Kolovsky, and H. J. Korsch, Phys. Lett. A **249**, 483 (1998).
[16] Y. V. Fyodorov and H. J. Sommers, J. Math. Phys. **38**, 1918 (1997).
[17] A. J. Lichtenberg and M. A. Lieberman, *Regular and Chaotic Dynamics* (Springer, Berlin, 1992); P. J. Bardroff, I. Bialynicki-Birula, D. S. Krämer, G. Kurizki, E. Mayr, P. Stifter, and W. P. Schleich, Phys. Rev. Lett. **74**, 3959 (1995).
[18] We note that the system (7) for $F = 0$, known as Double Resonance Model, is one of the chaos paradigm and has been intensively studied for last to decades both classically and quantum-mechanically (see [14] for references).
[19] F. T. Smith, Phys. Rev. **118**, 349 (1960).
[20] P. Seba, Phys. Rev. B **53**, 13024 (1996).
[21] P. Seba, K. Zyczkowski, and J. Zakrzewski, Phys. Rev. E **54**, 2438 (1996).
[22] V. A. Gopar, P. A. Mello, and M. Büttiker, Phys. Rev. Lett. **77**, 3005 (1996).
[23] M. Pozniak, K. Zyczkowski, and M. Kus, J.Phys. A: Math. Gen. **31**, 1059 (1998).
[24] To resolve the statistics one should go to smaller $\hbar$ and F, which would supply more data. Besides this, the limit $\hbar \to 0$ $F \to 0$ $(\hbar/F = rT/q)$ corresponds to $N \to \infty$ limit for the effective size (56) of the Floquet matrix. The latter limit was actually assumed in the analytical expressions given by RMT.
[25] M. V. Berry and M. Robnik, J. Phys. A: Math. Gen. **19**, 649 (1986); F. M. Izrailev, Phys. Rep. **196**, 299 (1990).